
DeNOTS: Stable Deep Neural ODEs for Time Series

Ilya Kuleshov¹ Evgenia Romanenkova¹ Vladislav Zhuzhel¹ Galina Boeva¹ Evgeni Vorsin² Alexey Zaytsev¹

Abstract

Neural ODEs are a prominent branch of methods designed to capture the temporal evolution of complex time-stamped data. Their idea is to solve an ODE with Neural Network-defined dynamics, which take the immediate parameters of the observed system into account. However, larger integration intervals cause instability, which forces most modern methods to normalize time to $[0, 1]$. We provably stabilize these models by introducing an adaptive negative feedback mechanism. This modification allows for longer integration, which in turn implies higher expressiveness, mirroring the behaviour of increasing depth in conventional Neural Networks. Additionally, it provides intriguing theoretical properties: forgetfulness and missing-value robustness. For three open datasets, our method obtains up to 20% improvements in downstream quality if compared to existing baselines, including State Space Models and Neural CDEs.

1. Introduction

Irregular time series are integral to numerous areas of modern life. Their analysis is a major direction of machine learning research. For example, global, sequence-wise downstream targets emerge for complex evolving systems related to patient sepsis (Reyna et al., 2020) and mortality (Johnson et al., 2016) prediction, pendulum dampening coefficient regression (Osin et al., 2024), pen tip trajectory character classification (Williams, 2006) and many others.

One of the most challenging aspects of these data is an uneven structure, which often requires sophisticated modifications to the processing algorithm. Specifically, recent works propose Neural Ordinary Differential Equations (ODEs) (Kidger et al., 2020) to account for irregularity naturally. Neural ODEs integrate a dynamics function represented by a Neural Network (NN), with linear transfor-

mations as its main building blocks. Consequently, NN integration may lead to exponential growth since this process is similar to integrating a matrix ODE with positive eigenvalues (Godunov, 1997). Without specific modifications, larger time frames consistently cause the methods' divergence, making them unusable for downstream tasks.

Most prior works deal with such exponential growth by considering time to be roughly $[0, 1]$, by setting it directly (Chen et al., 2018; Rubanova et al., 2019; Dupont et al., 2019), re-parametrizing it (Chen et al., 2020) or predicting it within tight bounds (Massaroli et al., 2020). Others devise models invariant to time transforms (Kidger et al., 2020). Existing works do not consider time to be an important hyperparameter. However, according to the original Neural ODE paper (Chen et al., 2018), the size of the integration interval corresponds to depth in traditional NNs. Deeper networks are more expressive, making long-interval integration worth fighting for.

Time series models possess another crucial property: we work with discrete observations instead of the true continuous process. The models cannot analyse the system during the resulting inter-observation gaps, accumulating epistemic uncertainty in the final representation (Blasco et al., 2024). Estimating such uncertainty has been a topic of interest for decades (Golubev & Krymova, 2013). Without additional modifications, it piles up with time, and the theoretical variance of the final prediction is proportional to sequence length. High variance makes the model vulnerable to adversarial attacks (Cohen et al., 2019).

Finally, time series often describe quickly evolving systems. To correctly model such objects, it is necessary to change the immediate representations swiftly (Bazarova et al., 2024a). Consequently, a model should pay close attention to the most recent tokens while retaining only general knowledge about the past, smoothing out specific details as time passes (Hochreiter & Schmidhuber, 1997). That said, it is important to maintain a balance between forgetting and remembering. Ideally, we seek a learnable, adaptive mechanism that would choose the ideal trade-off for each considered task, possibly even for each sample.

This work introduces DeNOTS — Stable Deep Neural ODEs for Time Series. Balancing the integration procedure via a negative feedback term in the derivative allows us

¹Skolkovo Institute of Science and Technology, Moscow, Russia ²Innotech, Moscow, Russia. Correspondence to: Ilya Kuleshov <i.kuleshov@skoltech.ru>.

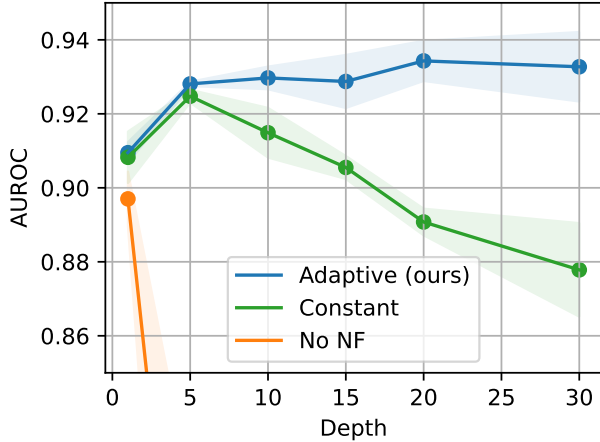


Figure 1. AUROC vs Depth (i.e. D from (4)) for DeNOTS on the Sepsis dataset, for our Adaptive (2) and Constant (3) (De Brouwer et al., 2019) versions of negative feedback, and the version without negative feedback (“No NF”).

to increase the integration depth while keeping the hidden trajectory from exploding uncontrollably. Moreover, using Gaussian Process theory, we prove that in our method, the aforementioned discretisation uncertainty does not accumulate in the final hidden state. Additionally, we establish that the influence of past observations decays. As depicted in Figure 1, it seems to preserve key prior knowledge through time: the model’s quality actually *increases* when we increase the time scale. In contrast, the existing negative feedback version from (De Brouwer et al., 2019) seems to “forget” important information with time, and the version with no negative feedback quickly diverges.

Overall, our contributions are as follows:

- The adaptive negative feedback mechanism, which provably bounds hidden trajectories of “deeper” models but does not limit the model’s flexibility in practice. Figure 1 demonstrates that only our version allows the model’s expressiveness to scale with depth.
- Gaussian Process-based analysis of the effect of discretisation on Neural CDE models, certifying that this uncertainty does not accumulate in our prediction. Experiments on increased fractions of missing values show that DeNOTS handles large inter-observation gaps well.
- Theoretical results, guaranteeing a forgetfulness property, which does not dispose of important past information. Empirically, DeNOTS is robust to beginning-of-sequence attacks while still accumulating knowledge throughout the sequence.
- An extensive experimental study of deeper Neural

ODEs, supporting the depth-time analogy, proposed by (Chen et al., 2018). We evaluate the novel method on three open datasets and compare it to modern baselines; DeNOTS excels in all settings.

2. Method

Representation learning for non-uniform time series.

We focus on solving downstream time series tasks with global, sequence-wise targets. Input is a sequence $S = \{(t_k, \mathbf{x}_k)\}_{k=1}^n$, where $t_k \in \mathbb{R}$ denotes time stamps and $\mathbf{x}_k \in \mathbb{R}^u$ are the feature-vectors of the corresponding observations. S is passed through the backbone to obtain an embedding $\mathbf{h} \in \mathbb{R}^v$, which, supposedly, characterises S as a whole. Finally, a linear head is used to transform \mathbf{h} into the prediction \hat{y} for the downstream problem, the form of which depends on the specific task we are solving. We consider binary or multiclass classification and regression problems.

The timestamps t_k often appear at irregular intervals. Conventional models, such as the Recurrent Neural Network (RNN) or the Transformer, tend to misinterpret these sequences, processing observations as if they lie on a uniform grid (Weerakody et al., 2021).

Neural ODE for sequential data. As we mentioned above, this issue can be elegantly solved by the use of ODEs. In short, we feed an interpolation of S to an NN, which is used as the dynamics function for an ODE. The value of this ODE’s solution at the final timestamp is taken to be the resulting representation \mathbf{h} . This means that our model evolves simultaneously with the observed system, taking in new observations as they happen in real-time. Formally, our method numerically integrates the following Cauchy problem:

$$\text{Dynamics: } \begin{cases} \mathbf{h}(t_1) = \mathbf{h}_0; \\ \frac{d\mathbf{h}(t)}{dt} = \mathbf{g}_\theta(\hat{\mathbf{x}}(t), \mathbf{h}(t)). \end{cases} \quad (1)$$

Solution: $\mathbf{h}(t) : [t_1, t_n] \rightarrow \mathbb{R}^u$.

Here, \mathbf{h}_0 is a predefined starting point, and \mathbf{g}_θ is a neural network, which defines the dynamics for $t \in [t_1, t_n]$. In our case, \mathbf{g} is a Gated Recurrent Unit (GRU) cell (Chung et al., 2014). The output of our backbone is the result of integrating these dynamics: $\mathbf{h} \equiv \mathbf{h}(t_n)$ — the value of the hidden trajectory at the final timestamp t_n .

This process requires a continuously-defined function $\mathbf{x}(t) : [t_1; t_n] \rightarrow \mathbb{R}^u$, instead of a discrete sequence $S = \{t_k, \mathbf{x}_k\}_{k=1}^n$. Following (Kidger et al., 2020), we reconstruct this data trajectory $\hat{\mathbf{x}}(t)$ via cubic splines:

$$\forall t \in [t_1, t_n], \hat{\mathbf{x}}(t) = \text{Spline}_S(t),$$

where Spline_S is a cubic spline, fitted to S .

Negative feedback. In contrast to prior work (Kidger et al., 2020), we carefully push the hidden trajectory towards zero by modifying the derivative to include *negative feedback*. Negative feedback solves the aforementioned instability issues that Neural ODEs face over longer timeframes. We subtract the current hidden state, possibly multiplied by a $[0, 1]$ weight, from the derivative. Specifically, in the last step of the GRU cell, we negate the term $\mathbf{z} \odot \mathbf{h}$ with the change highlighted in **red**:

$$\frac{d\mathbf{h}}{dt} = \text{GRU}(\hat{\mathbf{x}}(t), -\mathbf{h}(t)) = (1 - \mathbf{z}) \odot \mathbf{n} - \mathbf{z} \odot \mathbf{h}, \quad (2)$$

where \mathbf{z} is the output of a sigmoid-RNN layer, and \mathbf{n} is the output of a tanh-RNN layer from previous steps of the GRU. We implement it by passing $-\mathbf{h}$ instead of \mathbf{h} to the GRU. Alternatively, GRU-ODE-Bayes (De Brouwer et al., 2019) subtracts the current hidden state without any weight multipliers, resulting in:

$$\frac{d\mathbf{h}(t)}{dt} = (1 - \mathbf{z}) \odot (\mathbf{n} - \mathbf{h}). \quad (3)$$

Although \mathbf{z} is still present in this expression, it affects only the overall scale of the derivative without influencing the scale of the negative feedback term with respect to the updated state \mathbf{n} . Our fine-grained approach is more flexible. It does not constrain the resulting trajectory within $[-1, 1]$, as (3) does. Instead, in (2), \mathbf{z} depends on $\mathbf{h}(t)$ and $\mathbf{x}(t)$, so our negative feedback adapts to changes in these trajectories, remaining stable. Below, we will explore the stability of NF theoretically and its superior representative power in experiments.

Finally, adding negative feedback allows us to scale the integration interval:

$$t_k \leftarrow \frac{D}{M}(t_k - t_1), \text{ for } k = 1, \dots, n, \quad (4)$$

where $D > 0$ is a hyperparameter and $M > 0$ is a dataset-specific normalizing constant, introduced to make values of D comparable across benchmarks. According to (Chen et al., 2018), D corresponds to depth in traditional NN, and our experiments support this analogy. Without negative feedback, the hidden state suffers from exponential growth due to the nature of matrix differential equations, as we discuss in Section 3.2 and demonstrate in Section 4. Prior methods set integration boundaries around $[0, 1]$ as a regulariser (Chen et al., 2018; Dupont et al., 2019).

Our DeNOTS approach. The pseudocode for our approach is provided in Algorithm 1, complemented with an illustration in Figure 2. These artefacts sum up the inclusion of the negative feedback mechanism in Neural ODEs for sequential data.

Algorithm 1 The forward pass of DeNOTS. The backward pass is done via automatic differentiation.

INPUT:

\mathbf{h}_0 — embedding of static sequence features.
 $S \equiv \{(t_k, \mathbf{x}_k)\}_{k=1}^n$ — time series;
 $D > 0$ — depth hyperparameter;
 $M > 0$ — time normalizing constant;
 $\text{Spline}_S(\cdot)$ — cubic spline interpolation;
 $t_k \leftarrow \frac{D}{M}(t_k - t_1)$, for $k = 1, \dots, n$
 $\hat{\mathbf{x}}(\cdot) \leftarrow \text{Spline}_S(\cdot)$;

INTEGRATE:

INIT $\mathbf{h}(0) = \mathbf{h}_0$
 STEP $\frac{d\mathbf{h}}{dt} = \text{GRU}(\hat{\mathbf{x}}(t), -\mathbf{h}(t))$
 STOP $t \geq t_n$

RETURN: $\mathbf{h} \leftarrow \mathbf{h}(t_n)$

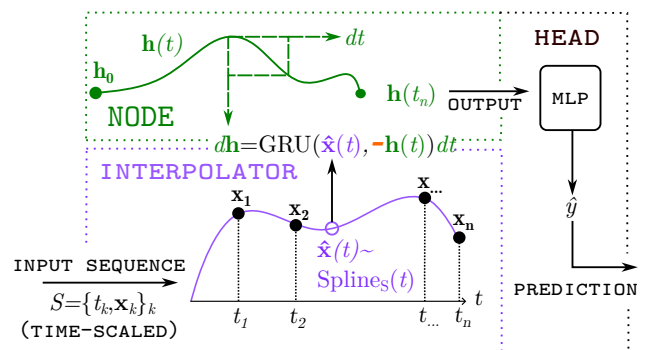


Figure 2. Scheme of the proposed DeNOTS method. The input sequence $\{t_k, \mathbf{x}_k\}_k$, after performing time-scaling (4), is passed into the backbone, where it is interpolated via cubic splines, and the result is then used to guide the Neural ODE trajectory. The large red minus sign ($-$) denotes our negative feedback mechanism. The final state of this trajectory is fed to a linear prediction head, which is responsible for solving the downstream task.

3. Theory

Due to space limitations, we leave out intermediate steps and proofs in this section. A more formal version with the necessary details is provided in Appendix A.

3.1. Preliminaries

We model our proposed backbone with the following ODE:

$$\frac{d\mathbf{h}}{dt} = \mathbf{f}_\theta(\hat{\mathbf{x}}(t), \mathbf{h}(t)) - W\mathbf{h}(t), \quad \hat{\mathbf{x}} \in \mathbb{R}^u, \mathbf{h} \in \mathbb{R}^v. \quad (5)$$

The values from (5) are constrained by an assumption:

Assumption 3.1. \mathbf{f} is Lipschitz w.r.t. both \mathbf{x} and \mathbf{h} :

$$\forall \mathbf{h}, \mathbf{x}, \mathbf{x}', \|\mathbf{f}_\theta(\mathbf{x}, \mathbf{h}) - \mathbf{f}_\theta(\mathbf{x}', \mathbf{h})\|_2 \leq L_x \|\mathbf{x} - \mathbf{x}'\|_2, \quad (6)$$

$$\forall \mathbf{x}, \mathbf{h}, \mathbf{h}', \|\mathbf{f}_\theta(\mathbf{x}, \mathbf{h}) - \mathbf{f}_\theta(\mathbf{x}, \mathbf{h}')\|_2 \leq L_h \|\mathbf{h} - \mathbf{h}'\|_2, \quad (7)$$

and the smallest eigenvalue λ of W is larger than the Lipschitz constant from (7), i.e. $L_h < \lambda$.

The form (5) is more convenient than (2). Simultaneously, we can show that it turns out to be more general:

Lemma 3.2. *Under Assumption 3.1, the GRU-based derivative from (2) is a special case of (5) if the l_2 norms of all the model’s weight matrices are small enough.*

The assumption of small weights, necessary to prove $L_h < \lambda$, holds in practice due to weight regularization. Below, we theoretically examine specific properties required from a neural ODE model, such as stability, forgetfulness, and robustness.

3.2. Stability

Intermediate states in NNs must be reasonably bounded for the model to learn due to the saturating nature of sigmoid, tanh and softmax activations (Ioffe & Szegedy, 2015). Neural ODE-based methods for time series are especially vulnerable to hidden-trajectory explosion. Indeed, it is well known that the solution of a linear ODE, defined by a matrix A , grows exponentially with time if at least one of its eigenvalues α_i is positive:

$$\frac{d\mathbf{h}}{dt} = A\mathbf{h} \implies \mathbf{h}(t) = \sum C_i \mathbf{v}_i e^{\alpha_i t}, \quad (8)$$

where α_i, \mathbf{v}_i are eigenvalues and eigenvectors of A , and $C_i > 0$ are arbitrary constants. Since NNs involve linear matrix multiplication, they also suffer from exponential growth, similar to (8). To the best of our knowledge, we are the first to raise this issue of long-timeframe integration and propose a provable solution to it.

To bound the hidden states of (5), we make the following assumption:

Assumption 3.3. $\hat{\mathbf{x}}(t)$ is l_2 -bounded:

$$\|\hat{\mathbf{x}}(t)\|_2 \leq C_x, \quad \forall t \in [t_1, t_n].$$

We can normalize and rescale the data at will, so the above holds in practice (Zucchet & Orvieto, 2024).

Using Assumption 3.3, we can formulate the Stability theorem:

Theorem 3.4. Stability. *Consider the Neural ODE (5) given Assumptions 3.1, 3.3. Then, $\|\mathbf{h}(t)\|_2$ is bounded:*

$$\forall t \in [t_1, t_n]: \|\mathbf{h}(t)\|_2 \leq \frac{L_x C_x + \|\mathbf{f}_\theta(\mathbf{0}_u, \mathbf{0}_v)\|_2}{\lambda - L_h},$$

where $\mathbf{0}_u, \mathbf{0}_v$ are zero-valued vectors of dimensions u, v respectively.

Theorem 3.4 implies that our negative feedback procedure provably prevents the norm of \mathbf{h} from increasing uncontrollably during integration.

3.3. Forgetfulness

For the considered problem of time series with global downstream targets, recent events usually hold the most relevant information about the sequence (Cao et al., 2019). So, the model should be able to forget unnecessary details and keep only essential knowledge. Our model provably satisfies this:

Theorem 3.5. Forgetfulness. *For the ODE (5) under Assumption 3.1 the following holds:*

$$\forall i \in \{1, \dots, v\}: \frac{d}{d\tau} \left\| \frac{d\mathbf{h}(t+\tau)}{dh_i(t)} \right\|_2 < 0,$$

i.e. the dependence of newer values of \mathbf{h} on all components of older values of \mathbf{h} decreases with time.

3.4. Robustness

The approximation $\hat{\mathbf{x}}(t)$ of the true unknown $\mathbf{x}(t)$ from discrete observations is a source of errors. We will measure how this uncertainty affects the quality of our final embedding $\mathbf{h}(t_n)$, assuming that $\mathbf{x}(t)$ is a realization of a Gaussian process (GP) (Kolmogorov, 1941; Stein, 2012). Importantly, the spline interpolation used in our algorithm and in (Kidger et al., 2020) is a specific case of Gaussian process regression (Golubev & Krymova, 2013).

Let $\mathbf{x}(t)$ be a stationary zero-mean u -dimensional GP with the covariance function $\mathbf{K}(\cdot, \cdot) = \{K_i(\cdot, \cdot)\}$ and independent components:

$$\begin{aligned} \mathbb{E}\mathbf{x}(t) &= \mathbf{0}, \\ \mathbb{E}[\mathbf{x}(t_1) \odot \mathbf{x}(t_2)] &= \mathbf{K}(t_1, t_2), \\ \mathbb{E}[x_i(t) \cdot x_j(t)] &= 0 \text{ for } i \neq j, \\ \mathbf{K}(t_1, t_2) &= \mathbf{K}(t_2 - t_1), \end{aligned} \quad (9)$$

where the symbol \odot denotes component-wise multiplication, and lower indexing x_i denotes vector components. Suppose we also know the values of \mathbf{x} at timestamps $\{t_1, \dots, t_n\} \subset \mathbb{R}$. Let $\hat{\mathbf{x}}(t)$ be the corresponding maximum a posteriori predictor (Kolmogorov, 1941). We introduce two types of uniform error bounds for convenience:

$$\sigma_{\text{PW}}^2 \triangleq \mathbb{E} \|\hat{\mathbf{x}}(t) - \mathbf{x}(t)\|_2^2; \quad \sigma_{\text{PW}}^2 \leq \bar{\sigma}_{\text{PW}}^2, \quad (10)$$

$$\sigma_{\text{INT}}^2 \triangleq \int_{t_k}^{t_{k+1}} \mathbb{E} \|\hat{\mathbf{x}}(t) - \mathbf{x}(t)\|_2^2 dt; \quad \sigma_{\text{INT}}^2 \leq \bar{\sigma}_{\text{INT}}^2, \quad (11)$$

where $\bar{\sigma}_{\text{INT}}, \bar{\sigma}_{\text{PW}}$ are the pointwise and the interval error bounds, constants independent of t and k . The expression (10) is more convenient; however, (11) can be derived for a wider class of covariance functions.

Most prior theoretic results are devised for the case of uniform sequences. To extend the bounds towards irregular data, we assume that changing interval sizes predictably changes the resulting error:

Assumption 3.6. Let $S = \{(t_k, \mathbf{x}_k)\}_k$ be a given irregular event sequence. We construct an alternative event sequence $\tilde{S} = \{(\tilde{t}_k, \mathbf{x}_k)\}_k$, with an additional margin r introduced between the m -th and $m + 1$ -th points:

$$\forall k \begin{cases} \tilde{t}_k = t_k, k \leq m; \\ \tilde{t}_k = t_k + r, k > m. \end{cases}$$

Consider the pointwise errors (10) for the original S and modified \tilde{S} sequences: σ^2 and $\tilde{\sigma}^2$, respectively. We assume they relate as follows:

$$\forall t \in \mathbb{R} \begin{cases} \sigma^2(t) \leq \tilde{\sigma}^2(\tilde{t}) & \text{for } r > 0, \\ \sigma^2(t) \geq \tilde{\sigma}^2(\tilde{t}) & \text{for } r < 0, \end{cases}$$

where $\tilde{t} = t + \mathbb{I}[t > t_{m+1}]r$, and \mathbb{I} denotes the indicator function.

The respective covariance determines the amount of information each observation provides about the unknown value. If all covariances decrease, the variance of $\hat{\mathbf{x}}$ will clearly increase and vice versa. We have also extensively tested this assumption empirically and provided a specific theoretical setting where this assumption provably holds in Appendix A.5. This allows us to expand uniform-sequence bounds towards bounds for irregular sequences by considering the minimum δ_{\min} or the maximum δ_{\max} step sizes.

We also make another common assumption:

Assumption 3.7. The input sequence is infinite:

$$k = -\infty, \dots, -2, -1, 0, 1, 2, \dots, +\infty.$$

Prior work (Zaytsev & Burnaev, 2017) demonstrated that the results for infinite sequences empirically hold for finite ones. Indeed, a typical kernel decays exponentially, so distant observations negligibly impact the resulting error.

Given these assumptions, we can estimate the error bounds. General expressions can be found in the Appendix. The following provides them for a common kernel function.

Lemma 3.8. *Under Assumptions 3.7, 3.6, for the squared exponential covariance function:*

$$\forall i = 1, \dots, u: K_i(t) = \sqrt{2\pi}e^{-2(\alpha\pi t)^2},$$

the interval error (11) for $\delta_{\min}\alpha \rightarrow 0, \delta_{\max}\alpha \rightarrow 0$ satisfies:

$$\begin{aligned} \sigma_{\text{INT}}^2 &\leq \bar{\sigma}_{\text{exp}}^{\max}(\delta_{\max}) \triangleq 7u\delta_{\max}^2\alpha \exp\left(-\frac{1}{8(\delta_{\max}\alpha)^2}\right), \\ \sigma_{\text{INT}}^2 &\geq \bar{\sigma}_{\text{exp}}^{\min}(\delta_{\min}) \triangleq \frac{4}{3}u\delta_{\min}^2\alpha \exp\left(-\frac{1}{8(\delta_{\min}\alpha)^2}\right). \end{aligned}$$

We will now estimate how much of the variance from (10) and (11) accumulates in the final hidden state. Consider a

version of (8), modified to account for $\hat{\mathbf{x}}$:

$$\frac{d\mathbf{h}}{dt} = A\mathbf{h}(t) + B\hat{\mathbf{x}}(t). \quad (12)$$

Equation (12) is a non-homogenous version of (8). Consequently, for reasonable values of B and $\hat{\mathbf{x}}$, it suffers from similar instability issues, exponentially accumulating the error from $\hat{\mathbf{x}}$.

As it turns out, our specific form of the hidden state derivative (5) inhibits its exponential growth, which is proved by the following theorem:

Theorem 3.9. Robustness (Gaussian Process standpoint). *Along with (5) under Assumption 3.1, consider analogous ODE dynamics for a realization of the actual Gaussian Process $\mathbf{x}(t)$ (instead of its MAP approximation $\hat{\mathbf{x}}(t)$):*

$$\begin{cases} \frac{d\mathbf{h}^*}{dt} = \mathbf{f}_\theta(\mathbf{x}(t), \mathbf{h}^*(t)) + W\mathbf{h}^*(t), \\ \mathbf{h}^*(t_1) = \mathbf{h}(t_1) = \mathbf{h}_0. \end{cases}$$

Then, depending on whether we are working with the pointwise (10) or the interval (11) errors, we can write different bounds on the variance, which accumulates in \mathbf{h} .

For the pointwise bound (10):

$$\mathbb{E}\|\mathbf{h}(t_n) - \mathbf{h}^*(t_n)\|_2^2 \leq \left(\frac{\bar{\sigma}_{PW}L_x}{\lambda - L_h}\right)^2. \quad (13)$$

For the interval bound (11):

$$\frac{1}{n} \int_{t_1}^{t_n} \mathbb{E}\|\mathbf{h}(t) - \mathbf{h}^*(t)\|_2^2 dt \leq \left(\frac{\bar{\sigma}_{INT}L_x}{\lambda - L_h}\right)^2. \quad (14)$$

The errors (13) and (14) do not depend on the number of observations. Consequently, uncertainty *does not accumulate in our final hidden state*.

3.5. Summary

We proved that our model (2) possesses the qualities of stability, forgetfulness and robustness. The validity of all three of these theorems directly depend on the presence of our negative feedback mechanism. In the general setting, without the $W\mathbf{h}$ term in (5), all of these results have counterexamples, as outlined by (8) and (12). We show below that negative feedback is also crucial for these properties in practice.

4. Experiments

In this section, we evaluate the quality of our model in comparison to state-of-the-art baselines. Also, we extensively study the declared properties of our novel negative feedback, which supposedly improves depth stability, expressiveness, robustness, and forgetfulness. Finer details of our experiments can be found in Appendix B.

Backbones. For baselines, we selected four most relevant architectures: the GRU Recurrent Neural Network (Chung et al., 2014), the Transformer with Rotary Positional Embeddings (Su et al., 2024), the state-space model Mamba (Gu & Dao, 2023), as well as the original Neural CDE (Kidger et al., 2020) model. Our DeNOTS model was tested in six versions: for depth $D = 1, 10, 20$, with or without negative feedback. Further details can be found in Appendix B.2. To investigate some baseline-specific artefacts we encountered in this benchmark, we provide a discussion section in Appendix B.7.2.

Datasets. We tested the aforementioned backbones on three open multivariate time series datasets: the PhysioNet Sepsis dataset (Reyna et al., 2020), the WISDM Human Activity Recognition (HAR) dataset (Weiss, 2019) and the synthetic Pendulum dataset, with the dampening coefficient as the target (Osin et al., 2024). Further details can be found in Appendix B.3. Due to space and computational time limitations, all follow-up experiments were conducted on one of these datasets. Dataset choice for each experiment is motivated in Appendix B.6.

4.1. Evaluation

Evaluation setting. Each experiment was run with three different seeds, and the results were averaged. The metrics for each considered dataset and model are presented in Table 1. Further details are provided in Appendix B.4.

| Backbone | HAR Acc. | Pendulum R^2 | Sepsis AUROC |
|-------------------|-------------|-------------------|-----------------|
| RNN | 0.38 | 0.49 | 0.86 |
| Transformer | 0.39 | <u>0.57</u> | 0.78 |
| SSM (Mamba) | 0.28 | <u>0.58</u> | 0.85 |
| NCDE | \times | -0.36 | 0.88 |
| DeNOTS-1 (No NF) | 0.47 | 0.47 | 0.90 |
| DeNOTS-10 (No NF) | 0.15 | \times | 0.45 |
| DeNOTS-20 (No NF) | 0.15 | \times | 0.44 |
| DeNOTS-1 | 0.48 | 0.44 | <u>0.91</u> |
| DeNOTS-10 | 0.39 | 0.63 | 0.93 |
| DeNOTS-20 | <u>0.43</u> | 0.64 | 0.93 |

Table 1. Main results on the three considered datasets. Best models are highlighted in **bold**, second-best are underlined, and a cross-mark (\times) indicates that the model did not converge. We present an average over three runs. A full version of this table with variances is in Table 4 from Appendix B. "DeNOTS- D " corresponds to the DeNOTS model with time scale D , and the "(No NF)" suffix means that we disabled negative feedback.

DeNOTS-20 beats the baselines on all datasets. However, we also provide some fine-grained conclusions and test them further with follow-up experiments.

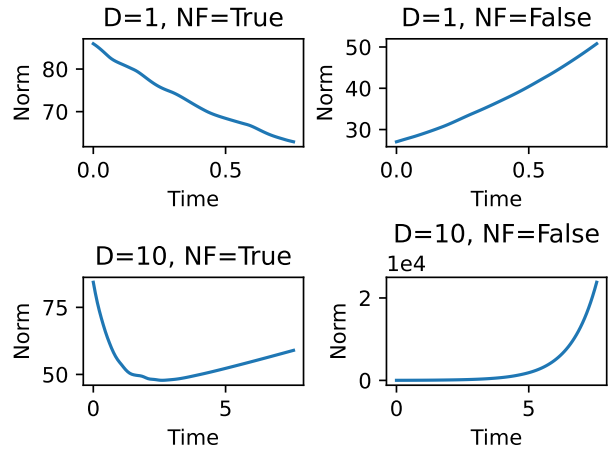


Figure 3. The l_2 norm of the hidden trajectory vs integration time, over the duration of the integration interval with (NF=True) and without (NF=False) negative feedback for depths $D = 1, 10$. Note the exponential multiplier $1e4$ for $D = 10$ with NF=False.

Depth Expressiveness. Both Sepsis and Pendulum show that increasing the depth of DeNOTS results in its better representation quality. However, the shallow $D = 1$ model outperforms others on HAR. We hypothesise this is due to the tiny size of the dataset: it has less than 1000 samples. So, we conduct a sensitivity study with a smaller version of Pendulum 1/32 the size of the original one. The results are in Table 2: the models with $D = 10, 20$ overfit with train R^2 scores 2-3 times higher than their test set counterparts. These deeper and more expressive versions are harmed by the additional flexibility, which causes overfitting (Hawkins, 2004).

| Timescale | Train R^2 | Test R^2 | Original R^2 |
|-----------|-----------------|-----------------|-----------------|
| $D = 1$ | 0.48 ± 0.05 | 0.31 ± 0.06 | 0.44 ± 0.01 |
| $D = 10$ | 0.69 ± 0.06 | 0.23 ± 0.04 | 0.63 ± 0.04 |
| $D = 20$ | 0.58 ± 0.07 | 0.19 ± 0.12 | 0.64 ± 0.04 |

Table 2. Train and test R^2 for a smaller version of Pendulum for overfitting identification. We present R^2 for the original dataset for convenience.

Stabilizing Effect of Negative Feedback. Without our negative feedback, DeNOTS diverges, showing abysmal performance for larger values of D . To illustrate the nature of this instability, we provide trajectory norm $\|\mathbf{h}(t)\|_2$ graphs in Figure 3. In line with our presumptions (8), without negative feedback, the norm grows exponentially with time, hampering downstream performance.

Negative Feedback Ablation. According to (2), our adaptive version of negative feedback (2) does not limit the hidden trajectory by superficial bounds, scaling the terms

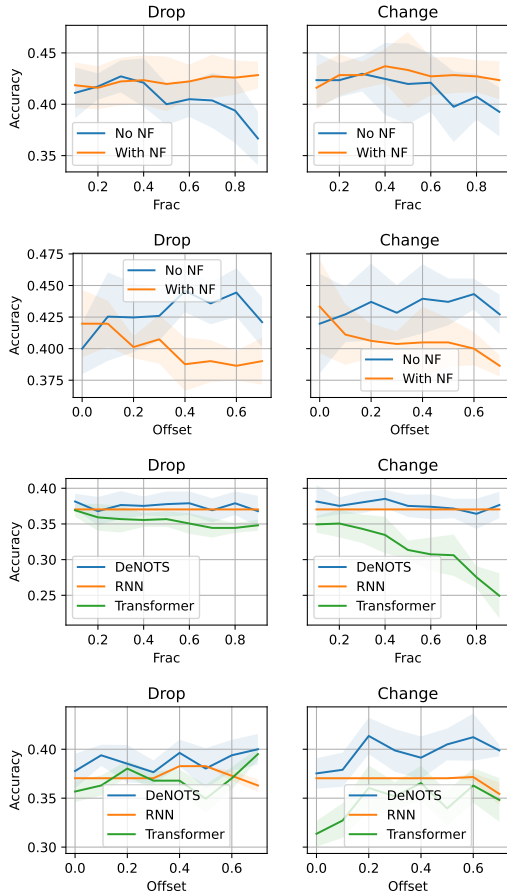


Figure 4. Adversarial attacks’ effects. We divided the models into two groups to ensure a fair comparison, investigated two attacks, and varied two hyperparameters, totalling eight graphs. The top half represents experiments with different versions of our method; bottom half — experiments with baseline methods. Left column — drop attack; right column — change attack. x -axis indicates the parameter we vary, “Frac” for the fraction of attack, “Offset” for the attack’s offset.

independently of each other, which makes it more versatile than the version presented in (3). In Figure 1, we compared it with the strict version (3) and the version without NF on Sepsis. Our approach is the only one that benefits from additional depth. The strict version (3) seems to scale poorly with D . It forces the hidden trajectory towards zero at a constant rate, which makes it hard for the model to retain prior knowledge on longer time frames.

4.2. Attacks

According to Theorems 3.5 and 3.9, our model is robust to certain attacks. We specifically consider change and drop attacks. In the *Change attack*, we add Gaussian noise to a fraction of the input sequence. Since we use batch normalisation, the Gaussian noise can be sampled from $\mathcal{N}(0, 1)$.

According to Theorem 3.5, the mistakes will supposedly be forgotten due to our negative feedback. In the *Drop attack*, we replace a fraction of the input sequence with NaNs. According to Theorem 3.9, larger inter-observation intervals imply larger Gaussian Process variance, which will not be accumulated in the final representation of our method. Both attacks have three hyperparameters: the size of the window to which the attack is localized, the offset of that window, and the fraction of tokens to attack in that window. We vary the offset and the fraction, fixing the size to 20% of the total sequence length.

All attack experiments were carried out on the HAR dataset since it’s the only one without NaNs, making it easier to work with. Following (Carlini et al., 2019), we study the robustness of our methods via perturbation curves, which provide an overall picture of attack efficiency for a range of hyperparameters. As a downside of this methodology, to ensure a correct comparison, we have to consider only those versions of the models which achieve similar metrics on plain, non-attacked data. This forces us to group the models by quality, investigating each group separately. The results are presented in Figure 4.

NF Sensitivity. The first group includes two versions of our model: DeNOTS-1 without NF and DeNOTS-20 with NF. We consider the $D = 1$ version of DeNOTS instead of the $D = 20$ to ensure convergence. Deeper models with NF perform better when attacks happen closer to the beginning of the sequence. However, as the attack’s offset increases, the quality of the negative feedback version drops. Without NF, the model is insensitive to attack location.

Baseline comparison. The second group of Figures compares DeNOTS-20 with NF with the baselines — RNN and the Transformer. As Mamba achieved very poor metrics, we could not include it fairly in this study. The DeNOTS-20 version, used in this baseline comparison, was trained for fewer epochs than that of the sensitivity study version, so its metrics on clean data are comparable to baselines’. In this case, our method remains robust regardless of the attack’s location or fraction of attacked tokens, retaining similar quality on plain data. In contrast, baselines degrade significantly: the Transformer is highly sensitive to the fraction of attacked tokens due to its equal focus on all sequence locations, and the RNN’s results are inconclusive.

Robustness summary. Independent of whether we drop or alter observations, the negative feedback version of our model is great at defending against beginning-of-sequence attacks in line with Theorems 3.5, 3.9: any past noise is forgotten, and long-interval variance does not accumulate throughout the sequence. If trained for fewer epochs, DeNOTS becomes even more robust while achieving RNN and

Transformer clean-data quality and outperforming Mamba.

5. Related works

Sequential Models. Plenty of deep-learning models exist for sequential data analysis. Base options include RNNs (Elman, 1991), along with their modifications for improving long-term memory, such as the GRU (Chung et al., 2014). However, these approaches still underperform on long-context tasks, and further research presents the attention mechanism to eliminate the issue altogether (Vaswani, 2017). Transformers, in turn, suffer from high computational costs: allocated memory scales quadratically with sequence length. State-space models, proposed recently, combine the benefits of Convolutional Networks and RNNs (Gu & Dao, 2023) while being significantly more efficient. Unfortunately, these works mostly ignore the irregular structure of the input sequences. Missing observations, which are common in time series, exacerbate this issue. Appending the time since the last observation to the feature vector and forward/backward filling seems to help (Osin et al., 2024); however, specialized methods are still preferred for this task (Kidger et al., 2020).

Neural ODEs for time-series. Neural ODEs provide an elegant way to take time into account. The representation evolves simultaneously with the observed system (Chen et al., 2018). For example, GRU-ODE-Bayes (De Brouwer et al., 2019) used Bayesian methods to account for missing observations optimally. To constrain the hidden trajectory to $[-1, 1]$, they introduced a basic version of negative feedback, subtracting the current hidden state from the derivative. Our work improves their strict negative feedback idea, proposing a gentler, adaptive solution: the bounds of our resulting trajectory are not fixed and, in effect, learned during training. This modification enhances the quality of the final representation according to our empirical study, especially on deeper models, i.e. ones with longer integration intervals — a topic which has not been explored previously.

As an improvement, the authors of (Kidger et al., 2020) proposed to combine Neural ODEs with the theory of Controlled Differential Equations (CDEs) (Friz & Victoir, 2010) for time series classification. Instead of embedding the input data into the starting point, Neural CDEs interpolate it, using the resulting function to guide the trajectory. In this paper, we also use splines to influence the derivative continuously.

On the other hand, Neural CDEs are not sensitive to the irregularity of time intervals (Kidger et al., 2020). So, the method appends the time difference as a separate feature. Moreover, these models have high memory usage. The controlling Neural Network has to generate a matrix, which implies a weight dimension of $\sim d^3$ (where d is the dimensionality of

the input features), instead of d^2 for conventional models, such as RNNs. Our model is more memory-efficient: the GRU cell as the dynamics function lowers memory consumption from $\sim d^3$ to $\sim d^2$. Besides, this makes our model sensitive to the input time intervals, which is crucial for increasing Neural ODE depth.

Gaussian process interpolation errors. Our theoretical analysis investigates discretisation uncertainty, which manifests itself as Gaussian Process variance. This involves estimating the squared error of an integral over a linear function of a Gaussian process with multiple outputs. For a specific assumption, we have a reasonable estimate of the quadratic risk that follows from (Golubev & Krymova, 2013). For the case of little knowledge about the smoothness of separate output dimensions, we can provide the minimax error estimation. This assumption leads us to generalise the results from (Golubev & Krymova, 2013; Zaytsev & Burnaev, 2017), where the authors considered a single output. While alternatives exist (Stein, 2012; van der Vaart & van Zanten, 2008; Zaytsev et al., 2018), they are unsuitable for the minimax setting described above with an additional ODE layer on top.

6. Conclusions

We proposed a novel ODE-based method for processing both regular and irregular time series, which incorporates negative feedback to deal with instability. According to our theoretical contributions, its hidden trajectory is bounded, discretisation uncertainty does not accumulate in the final representation, and the effect of older observations decays with time. Empirical studies show significant improvements from baseline methods w.r.t. quality and these robustness/forgetfulness properties. Although limited, the trajectory of DeNOTS remains flexible, and the model does not forget important knowledge about the past, only disposing of irrelevant details. Most importantly, unlike all other considered modifications, the quality of our method *improves* on larger integration intervals. This mimics the behaviour of deep conventional Neural Networks, supporting the depth-time analogy, which has not been tested before.

7. Limitations and Future Work

DeNOTS, like all Neural ODE methods, has a long execution time due to a high-level implementation; future work could develop faster differentiable ODE libraries. Additionally, it would be interesting to adapt our method of increasing depth in Neural ODEs to other domains, such as text, images, or tabular data.

Impact Statement

This work has the potential to significantly advance the application of Neural ODEs in domains where accurate modelling of complex, time-dependent systems is critical. Examples include healthcare, finance, and various models of the physical world. By enabling more stable and expressive methods that can handle larger integration intervals and missing data, this research allows more robust predictions and insights from real-world time-series data, which often exhibit irregularities and gaps.

From an ethical perspective, the ability to work with datasets that may be incomplete or noisy ensures that these models can be more reliably deployed in sensitive areas, such as medical diagnostics or environmental monitoring, where missing or imperfect data is common. For instance, in healthcare, better predictive models could lead to more timely interventions, improving patient outcomes and reducing costs.

However, with these advances come responsibilities. Deploying powerful predictive models in high-stakes fields raises concerns about transparency, accountability, and fairness. As these models become more integrated into decision-making processes, it is essential to ensure that they do not perpetuate biases or inequalities in data or outcomes. Future work must focus on making these models interpretable, ensuring that their predictions can be understood and trusted by non-experts and that they are designed to be fair and equitable across diverse populations.

Ultimately, the broader societal impact of DeNOTS could be significant, providing deeper continuous-depth models for addressing some of the world's most pressing challenges.

References

- Ansel, J. and team, P. . PyTorch 2: Faster Machine Learning Through Dynamic Python Bytecode Transformation and Graph Compilation. In *29th ACM International Conference on Architectural Support for Programming Languages and Operating Systems, Volume 2 (ASPLOS '24)*. ACM, April 2024.
- Bazarova, A., Kovaleva, M., Kuleshov, I., Romanenkova, E., Stepikin, A., Yugay, A., Mollaev, D., Kireev, I., Savchenko, A., and Zaytsev, A. Universal representations for financial transactional data: embracing local, global, and external contexts. *arXiv preprint arXiv:2404.02047*, 2024a.
- Bazarova, A., Romanenkova, E., and Zaytsev, A. Normalizing self-supervised learning for provably reliable change point detection. *arXiv preprint arXiv:2410.13637*, 2024b.
- Blasco, T., Sánchez, J. S., and García, V. A survey on uncertainty quantification in deep learning for financial time series prediction. *Neurocomputing*, 576:127339, 2024. ISSN 0925-2312.
- Cao, W., Ming, Z., Xu, Z., Zhang, J., and Wang, Q. Online sequential extreme learning machine with dynamic forgetting factor. *IEEE access*, 7:179746–179757, 2019.
- Carlini, N., Athalye, A., Papernot, N., Brendel, W., Rauber, J., Tsipras, D., Goodfellow, I., Madry, A., and Kurakin, A. On evaluating adversarial robustness. *arXiv preprint arXiv:1902.06705*, 2019.
- Chen, R. T., Rubanova, Y., Bettencourt, J., and Duvenaud, D. K. Neural ordinary differential equations. *Advances in NeurIPS*, 31, 2018.
- Chen, R. T., Amos, B., and Nickel, M. Neural spatio-temporal point processes. *arXiv preprint arXiv:2011.04583*, 2020.
- Chung, J., Gulcehre, C., Cho, K., and Bengio, Y. Empirical evaluation of gated recurrent neural networks on sequence modeling. In *NIPS 2014 Workshop on Deep Learning, December 2014*, 2014.
- Cohen, J., Rosenfeld, E., and Kolter, Z. Certified adversarial robustness via randomized smoothing. In *international conference on machine learning*, pp. 1310–1320. PMLR, 2019.
- De Brouwer, E., Simm, J., Arany, A., and Moreau, Y. Gru-ode-bayes: Continuous modeling of sporadically-observed time series. *Advances in NeurIPS*, 32, 2019.
- Dupont, E., Doucet, A., and Teh, Y. W. Augmented neural odes. *Advances in neural information processing systems*, 32, 2019.
- Elman, J. L. Distributed representations, simple recurrent networks, and grammatical structure. *Machine learning*, 7:195–225, 1991.
- Falcon, W. and The PyTorch Lightning team. PyTorch Lightning, March 2019.
- Friz, P. K. and Victoir, N. B. *Multidimensional stochastic processes as rough paths: theory and applications*, volume 120. Cambridge University Press, 2010.
- Godunov, S. K. *Ordinary differential equations with constant coefficient*, volume 169. American Mathematical Soc., 1997.
- Golubev, G. K. and Krymova, E. A. On interpolation of smooth processes and functions. *Problems of Information Transmission*, 49(2):127–148, 2013.

- Gu, A. and Dao, T. Mamba: Linear-time sequence modeling with selective state spaces. *arXiv preprint arXiv:2312.00752*, 2023.
- Hawkins, D. M. The problem of overfitting. *Journal of chemical information and computer sciences*, 44(1):1–12, 2004.
- Hochreiter, S. and Schmidhuber, J. Long short-term memory. *Neural computation*, 9(8):1735–1780, 1997.
- Ioffe, S. and Szegedy, C. Batch normalization: Accelerating deep network training by reducing internal covariate shift. In *Proceedings of The 32nd International Conference on Machine Learning*, pp. 448–456, 2015.
- Johnson, A. E., Pollard, T. J., Shen, L., Lehman, L.-w. H., Feng, M., Ghassemi, M., Moody, B., Szolovits, P., Anthony Celi, L., and Mark, R. G. Mimic-iii, a freely accessible critical care database. *Scientific data*, 3(1):1–9, 2016.
- Kidger, P., Morrill, J., Foster, J., and Lyons, T. Neural controlled differential equations for irregular time series. *Advances in NeurIPS*, 33:6696–6707, 2020.
- Kingma, D. P. Adam: A method for stochastic optimization. *arXiv preprint arXiv:1412.6980*, 2014.
- Kolmogorov, A. Interpolation and extrapolation of stationary random sequences. *Izvestiya Rossiiskoi Akademii Nauk. Seriya Matematicheskaya*, 5:3, 1941.
- Lienen, M. and Günnemann, S. torchode: A parallel ODE solver for pytorch. In *The Symbiosis of Deep Learning and Differential Equations II, NeurIPS*, 2022.
- Liu, J., Lin, Z., Padhy, S., Tran, D., Bedrax Weiss, T., and Lakshminarayanan, B. Simple and principled uncertainty estimation with deterministic deep learning via distance awareness. *Advances in neural information processing systems*, 33:7498–7512, 2020.
- Massaroli, S., Poli, M., Park, J., Yamashita, A., and Asama, H. Dissecting neural odes. *Advances in Neural Information Processing Systems*, 33:3952–3963, 2020.
- Osin, D., Udovichenko, I., Moskvoretskii, V., Shvetsov, E., and Burnaev, E. Ebes: Easy benchmarking for event sequences. *arXiv preprint arXiv:2410.03399*, 2024.
- Reyna, M. A., Josef, C. S., Jeter, R., Shashikumar, S. P., Westover, M. B., Nemati, S., Clifford, G. D., and Sharma, A. Early prediction of sepsis from clinical data: the physionet/computing in cardiology challenge 2019. *Critical care medicine*, 48(2):210–217, 2020.
- Rubanova, Y., Chen, R. T., and Duvenaud, D. K. Latent ordinary differential equations for irregularly-sampled time series. *Advances in NeurIPS*, 32, 2019.
- Stein, M. L. *Interpolation of spatial data: some theory for kriging*. Springer Science & Business Media, 2012.
- Su, J., Ahmed, M., Lu, Y., Pan, S., Bo, W., and Liu, Y. Roformer: Enhanced transformer with rotary position embedding. *Neurocomputing*, 568:127063, 2024.
- van der Vaart, A. and van Zanten, J. Rates of contraction of posterior distributions based on gaussian process priors. *Annals of Statistics*, 36(3):1435–1463, 2008.
- Vaswani, A. Attention is all you need. *Advances in Neural Information Processing Systems*, 2017.
- Weerakody, P. B., Wong, K. W., Wang, G., and Ela, W. A review of irregular time series data handling with gated recurrent neural networks. *Neurocomputing*, 441:161–178, 2021.
- Weiss, G. WISDM Smartphone and Smartwatch Activity and Biometrics Dataset. UCI Machine Learning Repository, 2019.
- Williams, B. Character Trajectories. UCI Machine Learning Repository, 2006.
- Yadan, O. Hydra - a framework for elegantly configuring complex applications. Github, 2019.
- Zaytsev, A. and Burnaev, E. Minimax approach to variable fidelity data interpolation. In *Artificial Intelligence and Statistics*, pp. 652–661. PMLR, 2017.
- Zaytsev, A., Romanenkova, E., and Ermilov, D. Interpolation error of gaussian process regression for misspecified case. In *Conformal and Probabilistic Prediction and Applications*, pp. 83–95. PMLR, 2018.
- Zucchet, N. and Orvieto, A. Recurrent neural networks: vanishing and exploding gradients are not the end of the story. *arXiv preprint arXiv:2405.21064*, 2024.

A. Theory

To enhance the reader experience, we duplicate all relevant statements and discussions from the main body in the Appendix, preserving reference numbering.

A.1. Preliminaries

We model our proposed backbone with the following ODE:

$$\frac{d\mathbf{h}}{dt} = \mathbf{f}_\theta(\hat{\mathbf{x}}(t), \mathbf{h}(t)) - W\mathbf{h}(t), \quad \hat{\mathbf{x}} \in \mathbb{R}^u, \mathbf{h} \in \mathbb{R}^v. \quad (5)$$

The following assumption defines the bounds for the values from (5):

Assumption (3.1). W from (5) is positive-definite, its smallest eigenvalue is λ , \mathbf{f} is Lipschitz w.r.t. both \mathbf{x} and \mathbf{h} :

$$\forall \mathbf{h}, \mathbf{x}, \mathbf{x}' : \|\mathbf{f}_\theta(\mathbf{x}, \mathbf{h}) - \mathbf{f}_\theta(\mathbf{x}', \mathbf{h})\|_2 \leq L_x \|\mathbf{x} - \mathbf{x}'\|_2, \quad (6)$$

$$\forall \mathbf{x}, \mathbf{h}, \mathbf{h}' : \|\mathbf{f}_\theta(\mathbf{x}, \mathbf{h}) - \mathbf{f}_\theta(\mathbf{x}, \mathbf{h}')\|_2 \leq L_h \|\mathbf{h} - \mathbf{h}'\|_2, \quad (7)$$

and the smallest eigenvalue of W is larger than the Lipschitz constant from (7), i.e. $L_h < \lambda$.

The form (5) is more convenient than (2). Simultaneously, as the following lemma shows, it turns out to be more general:

Lemma (3.2). *The GRU-based derivative from (2) under Assumption 3.1 is a special case of (5) if the l_2 norms of all the model's weight matrices are small enough.*

Proof. Let's show that equation (2) is a special case of (5). First, $W = \text{diag}(\mathbf{z})$, making it positive-definite. All the used activation functions (sigmoid and hyperbolic tangents) are Lipschitz-continuous, and so are linear layers (Liu et al., 2020; Bazarova et al., 2024b), so (6), (7) are also satisfied.

Last but not least, let's consider why the inequality $L_h < \lambda$ stands, in light of the model's weights being small: say, their l_2 norm is less than some $\varepsilon > 0$, and consider $\varepsilon \rightarrow 0$. As mentioned above, λ is represented by the output of a sigmoid \mathbf{z} , making it close to 0.5 for small parameter values:

$$\lambda = \sigma(\mathbf{p}) = \frac{1}{1 + e^{-\mathbf{p}}} = \frac{1}{2} + o(1),$$

where $\mathbf{p} = W_{hz}\mathbf{h} + W_{xz}\hat{\mathbf{x}} + \mathbf{b}$ also tends to zero, if $\varepsilon \rightarrow 0$:

$$\|W_{hz}\mathbf{h} + W_{xz}\hat{\mathbf{x}} + \mathbf{b}\|_2 \leq \|W_{hz}\| \|\mathbf{h}\| + \|W_{xz}\|_2 \|W_{xz}\| + \|\mathbf{b}\|_2 \leq \varepsilon(\|\mathbf{h}\| + \|\mathbf{x}\| + 1) \rightarrow 0.$$

On the other hand:

$$\mathbf{f} \equiv (1 - \mathbf{z}) \odot \mathbf{n},$$

where $\mathbf{z} \in [0, 1]$ as an output of a componentwise sigmoid layer. This implies that \mathbf{f} has a Lipschitz constant w.r.t. \mathbf{h} no larger than that of \mathbf{n} . Next, \mathbf{n} is a composition of hyperbolic tangents, which all have a Lipschitz constant of 1 and linear transformations with small norms:

$$\mathbf{n} = \tanh(W_{nx}\hat{\mathbf{x}} + \mathbf{b}_{nx} + \mathbf{r}(W_{nh}\mathbf{h} + \mathbf{b}_{nh})).$$

Since $\mathbf{r} \in [0, 1]$, again, as an out of a sigmoid, the Lipschitz constant of \mathbf{n} w.r.t. \mathbf{h} is no larger than that of W_{nh} . As is well known, the Lipschitz constant of a matrix is equal to its l_2 norm, meaning that the Lipschitz constant of \mathbf{f} is no greater than ε . Consequently,

$$\lambda = \frac{1}{2} + o(1) > \varepsilon > L_h, \quad \text{for } \|p\|_2 \rightarrow 0, \varepsilon \rightarrow 0.$$

□

A.2. Stability

To bound the hidden states of (5), we make the following assumption:

Assumption (3.3). $\hat{\mathbf{x}}(t)$ is l_2 -bounded:

$$\|\hat{\mathbf{x}}(t)\|_2 \leq C_x, \quad \forall t \in [t_1, t_n].$$

We can normalize and rescale the data at will, so the above holds in practice.

Using Assumption 3.3, we can formulate the Stability theorem:

Theorem (3.4). *Consider the task of modelling irregular sequences using a Neural ODE (5) under Assumptions 3.1, 3.3. Then, $\|\mathbf{h}(t)\|_2$ is bounded:*

$$\forall t \in [t_1, t_n], \|\mathbf{h}(t)\|_2 \leq \frac{L_x C_x + \|\mathbf{f}_\theta(\mathbf{0}_u, \mathbf{0}_v)\|_2}{\lambda - L_h},$$

where $\mathbf{0}_u, \mathbf{0}_v$ are zero-valued vectors of dimensions u, v respectively.

Proof. We start by considering the time-derivative of $\|\mathbf{h}\|_2^2$. It can be rewritten using the multiplication-derivative rule:

$$\begin{aligned} \frac{d}{dt} \|\mathbf{h}\|_2^2 &= 2 \left(\frac{d\mathbf{h}}{dt}, \mathbf{h} \right) = 2(\mathbf{f}_\theta(\hat{\mathbf{x}}(t), \mathbf{h}(t)) - W\mathbf{h}(t), \mathbf{h}) = \\ &= 2\mathbf{f}_\theta(\hat{\mathbf{x}}(t), \mathbf{h}(t))^T \mathbf{h} - 2\mathbf{h}^T W \mathbf{h} \leq 2 \|\mathbf{f}_\theta(\hat{\mathbf{x}}(t), \mathbf{h}(t))\|_2 \|\mathbf{h}\|_2 - 2\lambda \|\mathbf{h}\|_2^2. \end{aligned} \quad (15)$$

Next, we can bound the norm of \mathbf{f}_θ since it is Lipschitz (6), (7):

$$\begin{aligned} \|\mathbf{f}_\theta(\hat{\mathbf{x}}(t), \mathbf{h}(t))\|_2 &= \|\mathbf{f}_\theta(\hat{\mathbf{x}}(t), \mathbf{h}(t)) - \mathbf{f}_\theta(\mathbf{0}_u, \mathbf{0}_d) + \mathbf{f}_\theta(\mathbf{0}_u, \mathbf{0}_d)\|_2 \\ &\leq \|\mathbf{f}_\theta(\hat{\mathbf{x}}(t), \mathbf{h}(t)) - \mathbf{f}_\theta(\mathbf{0}_u, \mathbf{0}_d)\|_2 + \|\mathbf{f}_\theta(\mathbf{0}_u, \mathbf{0}_d)\|_2 \\ &\leq L_h \|\mathbf{h}(t)\|_2 + L_x \|\hat{\mathbf{x}}(t)\|_2 + \|\mathbf{f}_\theta(\mathbf{0}_u, \mathbf{0}_d)\|_2 \leq L_h \|\mathbf{h}(t)\|_2 + L_x C_x + \|\mathbf{f}_\theta(\mathbf{0}_u, \mathbf{0}_d)\|_2 \end{aligned}$$

where $\mathbf{0}_u, \mathbf{0}_d$ are zero-vectors of u and v dimensions respectively. This, together with (15), implies the following inequality:

$$\left(\frac{d\mathbf{h}}{dt}, \mathbf{h} \right) \leq (L_h - \lambda) \|\mathbf{h}\|_2^2 + (L_x C_x + \|\mathbf{f}_\theta(\mathbf{0}_u, \mathbf{0}_d)\|_2) \|\mathbf{h}\|_2.$$

This is a quadratic function of $\|\mathbf{h}\|_2$, and since $L_h < \lambda$, it turns negative for large enough $\|\mathbf{h}\|_2$. Putting it all together with (15):

$$\text{if } \|\mathbf{h}\|_2 > \frac{L_x C_x + \|\mathbf{f}_\theta(\mathbf{0}_u, \mathbf{0}_d)\|_2}{\lambda - L_h} \equiv C, \text{ then } \frac{d}{dt} \|\mathbf{h}\|_2 < 0,$$

which means that $\|\mathbf{h}\|_2$ is bounded by $C > 0$. □

A.3. Forgetfulness

Theorem (3.5). *For the ODE (5) under Assumption 3.1 the following holds:*

$$\forall i \in \{1, \dots, v\}, \frac{d}{d\tau} \left\| \frac{d\mathbf{h}(t+\tau)}{dh_i(t)} \right\|_2 < 0,$$

Proof. Without loss of generality, let's fix the index i . First, we can evidently reformulate the theorem's statement w.r.t. the square of the norm:

$$\frac{d}{d\tau} \left\| \frac{d\mathbf{h}(t+\tau)}{dh_i(t)} \right\|_2 < 0 \iff \frac{d}{d\tau} \left\| \frac{d\mathbf{h}(t+\tau)}{dh_i(t)} \right\|_2^2 < 0.$$

The square of the l_2 -norm can be re-written as the inner product:

$$\begin{aligned} \frac{d}{d\tau} \left\| \frac{d\mathbf{h}(t+\tau)}{dh_i(t)} \right\|_2^2 &= \frac{d}{d\tau} \left(\frac{d\mathbf{h}(t+\tau)}{dh_i(t)}, \frac{d\mathbf{h}(t+\tau)}{dh_i(t)} \right)_2 \\ &= 2 \left(\frac{d}{d\tau} \frac{d\mathbf{h}(t+\tau)}{dh_i(t)}, \frac{d\mathbf{h}(t+\tau)}{dh_i(t)} \right)_2. \end{aligned} \quad (16)$$

Since we are working with continuous functions, the derivatives can be swapped:

$$\begin{aligned} \frac{d}{d\tau} \frac{d\mathbf{h}(t+\tau)}{dh_i(t)} &= \frac{d}{dh_i(t)} \frac{d\mathbf{h}(t+\tau)}{d\tau} \\ &= \frac{d}{dh_i(t)} (\mathbf{f}_\theta(\mathbf{h}(t+\tau), \mathbf{x}(t+\tau)) + W\mathbf{h}(t+\tau)) \\ &\leq L_h\chi + W \frac{d\mathbf{h}(t+\tau)}{dh_i}, \end{aligned}$$

where $\chi \triangleq \left\| \frac{d\mathbf{h}(t+\tau)}{dh_i} \right\|_2$. Putting this together with (16), we achieve:

$$\frac{d}{d\tau} \left\| \frac{d\mathbf{h}(t+\tau)}{dh_i(t)} \right\|_2^2 \leq \left(L_h\chi + W \frac{d\mathbf{h}(t+\tau)}{dh_i}, \frac{d\mathbf{h}(t+\tau)}{dh_i} \right) \leq \chi^2(L_h - \lambda).$$

Since $L_h < \lambda$, this value is negative. □

A.4. Robustness

A.4.1. ASSUMPTIONS.

Let $\mathbf{x}(t)$ be a stationary zero-mean u -dimensional Gaussian process (GP) with the covariance function $\mathbf{K}(\cdot, \cdot) = \{K_i(\cdot, \cdot)\}$ and independent components:

$$\begin{aligned} \mathbb{E}\mathbf{x}(t) &= \mathbf{0}, \\ \mathbb{E}[\mathbf{x}(t_1) \odot \mathbf{x}(t_2)] &= \mathbf{K}(t_1, t_2), \\ \mathbb{E}[x_i(t) \cdot x_j(t)] &= 0 \text{ for } i \neq j, \\ \mathbf{K}(t_1, t_2) &= \mathbf{K}(t_2 - t_1), \end{aligned} \tag{9}$$

where the symbol \odot denotes component-wise multiplication, and lower indexing x_i denotes vector components.

Suppose we also know the values of the process from (9) at timestamps $\{t_1, \dots, t_n\} \subset \mathbb{R}$. Consider the corresponding maximum a posteriori predictor $\hat{\mathbf{x}}(t)$:

$$\hat{\mathbf{x}}(t) = \underset{\mathbf{x}(t)}{\operatorname{argmax}} p[\mathbf{x}(t) | \mathbf{x}(t_1) = \mathbf{x}_1, \dots, \mathbf{x}(t_n) = \mathbf{x}_n].$$

We seek to devise two types of uniform error bounds for the predictor:

$$\sigma_{\text{PW}}^2 \triangleq \mathbb{E} \|\hat{\mathbf{x}}(t) - \mathbf{x}(t)\|_2^2; \quad \sigma_{\text{PW}}^2 \leq \bar{\sigma}_{\text{PW}}^2, \tag{10}$$

$$\sigma_{\text{INT}}^2 \triangleq \int_{t_k}^{t_{k+1}} \mathbb{E} \|\hat{\mathbf{x}}(t) - \mathbf{x}(t)\|_2^2 dt; \quad \sigma_{\text{INT}}^2 \leq \bar{\sigma}_{\text{INT}}^2. \tag{11}$$

We refer to $\bar{\sigma}_{\text{PW}}$, $\bar{\sigma}_{\text{INT}}$ as the pointwise and the interval upper error bounds, respectively. The expression (10) is more convenient; however, (11) can be derived for a wider class of covariance functions, so we use both.

To simplify the analysis, we make two assumptions about the nature of the sequences we are working with. However, they do not limit the applicability of our results.

Most prior theoretic results are devised for the case of uniform sequences. To extend the bounds towards irregular data, we assume that changing interval sizes predictably changes the resulting error:

Assumption (3.6). Let $S = \{(t_k, \mathbf{x}_k)\}_k$ be a given irregular event sequence. We construct an alternative event sequence $\tilde{S} = \{(\tilde{t}_k, \mathbf{x}_k)\}_k$, with an additional margin r introduced between the m -th and $m+1$ -th points:

$$\forall k \begin{cases} \tilde{t}_k = t_k, k \leq m; \\ \tilde{t}_k = t_k + r, k > m. \end{cases}$$

Consider the pointwise errors (10) for the original S and modified \tilde{S} sequences: σ^2 and $\tilde{\sigma}^2$, respectively. We assume they relate as follows:

$$\forall t \in \mathbb{R} \quad \begin{cases} \sigma^2(t) \leq \tilde{\sigma}^2(\tilde{t}) & \text{for } r > 0, \\ \sigma^2(t) \geq \tilde{\sigma}^2(\tilde{t}) & \text{for } r < 0, \end{cases}$$

where $\tilde{t} = t + \mathbb{I}[t > t_{m+1}]r$, and \mathbb{I} denotes the indicator function.

The respective covariance determines the amount of information each observation provides about the unknown value. If all covariances decrease, the variance of $\hat{\mathbf{x}}$ will clearly increase and vice versa. We have also extensively tested this assumption empirically and consider a specific theoretical setting where this assumption holds. The details can be found in Appendix A.5.

Assumption 3.6 is formulated for pointwise errors (10), however similar conclusions for interval errors (11) follow as corollaries:

Corollary A.1. *Under the notation of Assumption 3.6, the corresponding interval errors relate similarly:*

$$\forall k \quad \begin{cases} \sigma_k^2 \leq \tilde{\sigma}_k^2 & \text{for } r > 0, \\ \sigma_k^2 \geq \tilde{\sigma}_k^2 & \text{for } r < 0. \end{cases}$$

Finally, we can extend all the devised error bounds towards irregular sequences.

Corollary A.2. *Consider an irregular time series $S = \{(t_k, \mathbf{x}_k)\}$. Let $\delta_{\min}, \delta_{\max}$ be the minimum and maximum intervals between observations of S , respectively:*

$$\begin{aligned} \delta_{\min} &= \min_k (t_k - t_{k-1}), \\ \delta_{\max} &= \max_k (t_k - t_{k-1}). \end{aligned}$$

Consider also two regular sequences, with $\delta_{\min}, \delta_{\max}$ as the inter-observation intervals:

$$\begin{aligned} S_{\min} &= \{(k\delta_{\min}, \mathbf{x}_k)\}_k, \\ S_{\max} &= \{(k\delta_{\max}, \mathbf{x}_k)\}_k. \end{aligned}$$

Then, under the assumption 3.6, their interval errors (11) relate as follows:

$$\sigma_{\min,INT}^2 \leq \sigma_k^2 \leq \sigma_{\max,INT}^2 \quad \forall k.$$

We also make another common assumption:

Assumption (3.7). The input sequence is infinite:

$$k = -\infty, \dots, -2, -1, 0, 1, 2, \dots, +\infty.$$

Prior work (Zaytsev & Burnaev, 2017) demonstrated that the results for infinite sequences empirically hold for finite ones. Indeed, since a typical kernel decays with an exponential speed, distant observations negligibly impact the resulting error.

A.4.2. ERROR BOUNDS.

In this section, we will work under the uniform-grid assumption: according to Corrolary A.2, all the results devised under this assumption can be extended to irregular sequences:

Assumption A.3. The sequence S is uniform:

$$t_{k+1} - t_k = \delta, \quad \forall k.$$

The optimal estimator for a uniform infinite grid is well-known (Kolmogorov, 1941):

$$\hat{\mathbf{x}}(t) = \delta \sum_{k=-\infty}^{\infty} \mathbf{K}(t - k\delta) \odot \mathbf{x}(k\delta), \quad (17)$$

where optimal $\hat{\mathbf{K}}$ is a symmetric kernel that depends on a spectral density. This form allows us to deduce analytical error bounds. For this purpose, we generalize the results from (Zaytsev & Burnaev, 2017) to multiple dimensions. This is given by the following lemma.

Lemma A.4. *Let $\mathbf{F}(\omega)$ denote the spectral density of Gaussian process from (9):*

$$\mathbf{F}(\omega) = \int_{-\infty}^{\infty} \exp(2\pi i\omega t) \mathbf{K}(t) dt.$$

In this notation, under Assumptions A.3,3.7, and if all components of \mathbf{K} are equal, the following holds:

$$\mathbb{E}\|\hat{\mathbf{x}}(t) - \mathbf{x}(t)\|^2 = u \int_{-\infty}^{\infty} F(\omega) \left| 1 - \sum_{k \neq 0} e^{2i\pi\omega(t-t_k)} K(t-t_k) \right|^2 d\omega,$$

where $K(t) \equiv K_i(t)$ and $F(\omega) \equiv F_i(\omega)$ are the components of the kernel function and the spectral density, respectively.

Proof. Let us start with expanding the square:

$$\mathbb{E}\|\hat{\mathbf{x}}(t) - \mathbf{x}(t)\|^2 = \mathbb{E}[\hat{\mathbf{x}}^T(t)\hat{\mathbf{x}}(t)] - 2\mathbb{E}[\hat{\mathbf{x}}^T(t)\mathbf{x}(t)] + \mathbb{E}[\mathbf{x}^T(t)\mathbf{x}(t)].$$

Now, we consider the terms one by one, substituting (17) and rewriting in terms of spectral density. The first term gives:

$$\begin{aligned} \mathbb{E}[\hat{\mathbf{x}}^T(t)\hat{\mathbf{x}}(t)] &= h^2 u \sum_{k,l=-\infty}^{\infty} K(t-t_k)K(t-t_l)K(t_k-t_l) = \\ &= \int_{-\infty}^{\infty} F(\omega) \left(h^2 u \sum_{k=-\infty}^{\infty} K(t-t_k)K(t-t_l)e^{2\pi i\omega(t_l-t_k)} \right) d\omega. \end{aligned}$$

The second one:

$$\begin{aligned} 2\mathbb{E}[\hat{\mathbf{x}}^T(t)\mathbf{x}(t)] &= 2hu \sum_{k=-\infty}^{\infty} K^2(t-t_k) = \\ &= \int_{-\infty}^{\infty} F(\omega) \left(2hu \sum_{k=-\infty}^{\infty} K(t-t_k)e^{2\pi i\omega(t-t_k)} \right) d\omega. \end{aligned}$$

And, finally, the third one:

$$\mathbb{E}[\mathbf{x}^T(t)\mathbf{x}(t)] = K(0)u = u \int_{-\infty}^{\infty} F(\omega) d\omega.$$

Factoring out the spectral density integral, the remaining three terms are the expansion of the following modulus:

$$u \left| 1 + h \sum_{k=-\infty}^{\infty} K(t-t_k)e^{2\pi i\omega(t-t_k)} \right|^2.$$

□

With Lemma A.4, all other results can be taken directly from (Zaytsev & Burnaev, 2017), taking into account that $\mathbf{x}(t)$ is u -dimensional. We recount select findings from this paper: the general error form, an analytic error expression for a specific kernel and the minimax error bound.

Theorem A.5. Under the assumptions from Lemma A.4, the error σ_{INT}^2 from (11), may be written in the following form:

$$\sigma_{INT}^2 = u\delta \int_{-\infty}^{\infty} F(\omega) \left((1 - \hat{K}(\omega))^2 + \sum_{k=-\infty}^{\infty} \hat{K}\left(\omega + \frac{k}{\delta}\right) \right) d\omega, \quad (18)$$

where \hat{K} is the Fourier transform of K .

Note that the error (18) does not depend on the interval number. This is due to the inherent symmetry of an infinite uniform grid: all intervals are the same from the perspective of the covariance function.

We also devise the bounds for a specific common kernel function.

Assumption A.6. The covariance function is the same for all dimensions and corresponds to the squared exponential function:

$$K(t) = \sqrt{2\pi} e^{-2(\alpha\pi t)^2}.$$

The following corollary is rewritten in terms of Corollary A.2 to be compatible with the main-text version.

Corollary (Lemma 3.8). Under the Assumptions 3.7, A.3, A.6, the interval error (18) for $\delta_{\min}\alpha \rightarrow 0, \delta_{\max}\alpha \rightarrow 0$ satisfies:

$$\begin{aligned} \sigma_{INT}^2 &\leq \bar{\sigma}_{\text{exp}}^{\max}(\delta_{\max}) \triangleq 7u\delta_{\max}^2\alpha \exp\left(-\frac{1}{8(\delta_{\max}\alpha)^2}\right), \\ \sigma_{INT}^2 &\geq \bar{\sigma}_{\text{exp}}^{\min}(\delta_{\min}) \triangleq \frac{4}{3}u\delta_{\min}^2\alpha \exp\left(-\frac{1}{8(\delta_{\min}\alpha)^2}\right). \end{aligned}$$

On the other hand, we may also use a more general approach to determining the covariance function \mathbf{K} , independent of the specific kernel, since it may be unknown or may vary between dimensions. It leads us to the following Assumption:

Assumption A.7. All the spectral densities of \mathbf{K} belong to the following class of functions:

$$\mathcal{F}(L) = \left\{ F : \mathbb{E} \left(\frac{\partial x_F(t)}{\partial t} \right)^2 \leq L \right\}. \quad (19)$$

Then, we can generalize results from (Zaytsev & Burnaev, 2017) for the multivariate case.

Theorem A.8. In the above notation, under the Assumptions 3.7, A.3, A.7, the minimax GP interpolation error may be calculated analytically:

$$R^h(L) \triangleq \inf_{\tilde{\mathbf{x}}} \sup_{F \in \mathcal{F}(L)} \sigma_{INT}^2 = \frac{L\delta^2 u}{2\pi^2}. \quad (20)$$

Finally, using the above bounds, we can write corresponding expressions for the final hidden state of DeNOTS.

Theorem (3.9). Robustness (Gaussian Process standpoint). Along with (5) under Assumption 3.1, consider analogous ODE dynamics for a realization of the actual Gaussian Process $\mathbf{x}(t)$ (instead of its MAP approximation $\tilde{\mathbf{x}}(t)$):

$$\begin{cases} \frac{d\mathbf{h}^*}{dt} = \mathbf{f}_\theta(\mathbf{x}(t), \mathbf{h}^*(t)) + W\mathbf{h}^*(t), \\ \mathbf{h}^*(t_1) = \mathbf{h}(t_1) = \mathbf{h}_0. \end{cases}$$

Then, depending on whether we are working with the point-wise (10) or the interval (11) errors, we can write different bounds on the variance, which accumulates in \mathbf{h} .

For the pointwise bound (10):

$$\mathbb{E} \|\mathbf{h}(t_n) - \mathbf{h}^*(t_n)\|_2^2 \leq \left(\frac{\bar{\sigma}_{\text{PW}} L_x}{\lambda - L_h} \right)^2.$$

For the interval bound (11):

$$\frac{1}{n} \int_{t_1}^{t_n} \mathbb{E} \|\mathbf{h}(t) - \mathbf{h}^*(t)\|_2^2 dt \leq \left(\frac{\bar{\sigma}_{\text{INT}} L_x}{\lambda - L_h} \right)^2.$$

Proof. Consider the time-derivative of the squared error norm, multiplied by $\frac{1}{2}$ for convenience:

$$\begin{aligned}
 \frac{1}{2} \frac{d}{dt} \|\mathbf{h}(t) - \mathbf{h}^*(t)\|_2^2 &= \left(\frac{d(\mathbf{h}(t) - \mathbf{h}^*(t))}{dt}, \mathbf{h}(t) - \mathbf{h}^*(t) \right) = \\
 &= (\mathbf{f}_\theta(\hat{\mathbf{x}}(t), \mathbf{h}(t)) - \mathbf{f}_\theta(\mathbf{x}(t), \mathbf{h}^*(t)) - W(\mathbf{h}(t) - \mathbf{h}^*(t)), \mathbf{h}(t) - \mathbf{h}^*(t)) = \\
 &= (\mathbf{f}_\theta(\hat{\mathbf{x}}(t), \mathbf{h}(t)) - \mathbf{f}_\theta(\mathbf{x}(t), \mathbf{h}^*(t)), \delta\mathbf{h}(t)) - \delta\mathbf{h}^T(t)W\delta\mathbf{h}(t) = \\
 &\leq L_h \|\delta\mathbf{h}\|_2^2 + L_x \|\delta\mathbf{x}(t)\|_2 \|\delta\mathbf{h}\|_2 - \lambda \|\delta\mathbf{h}\|_2^2 = \\
 &= (L_h - \lambda) \|\delta\mathbf{h}\|_2^2 + L_x \|\delta\mathbf{x}(t)\|_2 \|\delta\mathbf{h}\|_2, \tag{21}
 \end{aligned}$$

where we introduce the following notation for conciseness:

$$\begin{aligned}
 \delta\mathbf{h}(t) &\triangleq \mathbf{h}(t) - \mathbf{h}^*(t), \\
 \delta\mathbf{x}(t) &\triangleq \hat{\mathbf{x}}(t) - \mathbf{x}(t).
 \end{aligned}$$

If we have a pointwise bound on $\mathbb{E} \|\delta\mathbf{x}(t)\|^2$, the expression from (21) can be upper bounded by a quadratic function, where the multiplier $L_h - \lambda$ next to the squared term is negative, since $L_h < \lambda$. It turns negative for larger $\|\delta\mathbf{h}(t)\|_2$:

$$\text{if } \|\delta\mathbf{h}\|_2 > \frac{L_x \bar{\sigma}_{\text{PW}}}{\lambda - L_h}, \text{ then } (L_h - \lambda) \|\delta\mathbf{h}(t)\|_2^2 + L_x \sigma_{\text{PW}} \|\delta\mathbf{h}(t)\|_2 < 0 \implies \frac{1}{2} \mathbb{E} \frac{d}{dt} \|\mathbf{h}(t) - \mathbf{h}^*(t)\|_2^2 \leq 0, \tag{22}$$

which proves half of this theorem.

However, if we only have an interval error bound, we are forced to integrate (21) on an interval $[t_1, t_k]$ for some $k \in \mathbb{N}$:

$$\frac{1}{2} \int_{t_1}^{t_k} \frac{d}{dt} \|\mathbf{h}(t) - \mathbf{h}^*(t)\|_2^2 dt \leq \int_{t_1}^{t_k} \|\delta\mathbf{h}(t)\|_2^2 (L_h - \lambda) dt + \int_{t_1}^{t_k} L_x \|\delta\mathbf{x}(t)\|_2 \|\delta\mathbf{h}(t)\|_2 dt. \tag{23}$$

Let us rewrite the last term, dropping all constants, and use the Cauchy–Schwartz inequality for integrals:

$$\int_{t_1}^{t_k} \|\delta\mathbf{x}(t)\|_2 \|\delta\mathbf{h}(t)\|_2 dt \leq \sqrt{\int_{t_1}^{t_k} \|\delta\mathbf{x}(t)\|_2^2 dt \int_{t_1}^{t_k} \|\delta\mathbf{h}(t)\|_2^2 dt} \triangleq XH\sqrt{k},$$

where we introduced the following notation:

$$X^2 \triangleq \int_{t_1}^{t_k} \|\delta\mathbf{x}(t)\|_2^2 dt, \quad H^2 \triangleq \int_{t_1}^{t_k} \|\delta\mathbf{h}(t)\|_2^2 dt.$$

In light of that, let's rewrite (23):

$$\frac{1}{2} (\|\delta\mathbf{h}(t_k)\|_2^2 - \|\delta\mathbf{h}(t_1)\|_2^2) = \frac{1}{2} \|\delta\mathbf{h}(t_k)\|_2^2 \leq (L_h - \lambda)H^2 + L_x XH\sqrt{k}.$$

The right-hand side is a quadratic function w.r.t. H , and, again, the multiplier next to the squared term is negative. Simultaneously, the left-hand side is positive, being a norm. Together, this means that H needs to be in between the roots of this quadratic function to satisfy the positivity constraints:

$$0 \leq H \leq \frac{L_x X \sqrt{k}}{\lambda - L_h}.$$

Taking the expectation of the square and factoring in the interval bound, which transforms into $\mathbb{E}X^2 \leq \bar{\sigma}_{\text{NT}}^2$ due to linearity, we conclude the proof. \square

A.5. Validation of Assumption 3.6.

The assumption was tested for the common quadratic kernel:

$$K(\delta t) = e^{-(\delta t)^2/2}.$$

The procedure is outlined in algorithm 2 and is also available as a Python script in our paper’s repository. It randomly chooses sequence length, sequence times, displacement amount and location and calculates the variance of a Gaussian Process fitted to the generated sequence at a random time. Finally, it asserts that the sequence with increased intervals has an error bigger than the initial one. The loop successfully runs for 1000 iterations, suggesting that the hypothesis typically holds under natural settings.

Now, let us consider a typical theoretical dynamic of the posterior error variance for the point prediction with minimum variance under standard Gaussian process assumptions.

Denote by $\mathcal{D}_{a,b,\delta}$ for positive integer a and b a set of points $\{-\infty, \dots, -(a+1)\delta, -a\delta, b\delta, (b+1)\delta, \dots, +\infty\}$. For each design of experiments $\mathcal{D}_{a,b,\delta}$ we have a corresponding sample of pairs $D_{a,b,\delta} = \{(t, \mathbf{x}(t))\}_{t \in \mathcal{D}_{a,b,\delta}}$. Then, for a specific t we can define $\sigma_{\text{PW},D}^2(t) = \min_{\hat{\mathbf{x}}} \mathbb{E}(\|\hat{\mathbf{x}} - \mathbf{x}(t)\|_2^2 | D)$, there by $\mathbb{E}(\cdot | D)$ we denote mean of a random variable given the sample D . Then, the following Lemma holds.

Lemma A.9. *Let us consider two design of experiments $\mathcal{D}_{a_1,b_1,\delta}$ and $\mathcal{D}_{a_2,b_2,\delta}$ with corresponding samples $D_1 = D_{a_1,b_1,\delta}$ and $D_2 = D_{a_2,b_2,\delta}$ that take values of $\mathbf{x}(t)$ from the same realization of a Gaussian process.*

Suppose that $a_2 \geq a_1$ and $b_2 \geq b_1$. Then

$$\sigma_{\text{PW},D_1}^2(t) \leq \sigma_{\text{PW},D_2}^2(t).$$

Proof. Given the correspondence between a_1, a_2, b_1, b_2 , it holds that $\mathcal{D}_{a_2,b_2,\delta} \subseteq \mathcal{D}_{a_1,b_1,\delta}$. So, for $\sigma_{\text{PW},D_1}^2(t) = \min_{\hat{\mathbf{x}}} \mathbb{E}(\|\hat{\mathbf{x}} - \mathbf{x}(t)\|_2^2 | D_1)$ we have additional observations of our Gaussian process. Thus, this variance for D_1 would decrease or at least stay the same. \square

This Lemma provides an intuition that we aim for: for more distant observations, the expected quadratic error is higher. If we make observations closer, we instead obtain a better model.

Algorithm 2 Monte Carlo hypothesis testing.

loop

$n \leftarrow \text{randint}(5, 300)$

$r \leftarrow \text{rand}()$

mark iteration-start

$\{t_k\}_{k=1}^n \leftarrow \text{sort}(\text{rand}(n))$

$t_1 \leftarrow 0$

$t_n \leftarrow 1$

$i \leftarrow \text{randint}(1, N - 1)$

$\{\tilde{t}_k\}_k \leftarrow \{t_1, \dots, t_{i-1}, t_i + r, \dots, t_n + r\}$

$K \leftarrow \text{cov}(\{t_i - t_j\}_{i,j})$

$\tilde{K} \leftarrow \text{cov}(\{\tilde{t}_i - \tilde{t}_j\}_{i,j})$

$t \leftarrow \text{rand}()$

$\tilde{t} \leftarrow t$

if $t_i < t$ **then**

$\tilde{t} \leftarrow t + r$

end if

if Singular(K) **or** Singular(\tilde{K}) **then**

goto iteration-start

end if

$k \leftarrow \text{cov}(\{t_k - t\}_k)$

$\tilde{k} \leftarrow \text{cov}(\{\tilde{t}_k - \tilde{t}\}_k)$

$D \leftarrow \text{cov}(0) - \text{quad}(K, k)$

$\tilde{D} \leftarrow \text{cov}(0) - \text{quad}(\tilde{K}, \tilde{k})$

assert $D < \tilde{D}$

end loop

B. Experiment Details

B.1. Reproducibility

All of the datasets, models, and libraries used are open and publicly available. We also publish our repository online ¹. It contains automated scripts for data downloading, preprocessing, and for model training. All hyperparameters are also made available in the form of YAML configs and included in our repository. The documentation clearly explains the steps necessary to reproduce all considered experiments.

B.2. Backbones

All the considered models are small, with hidden sizes fixed to 32 and the number of layers fixed to 1 (where applicable). This is done deliberately to facilitate reproducibility and reduce experimentation time.

DeNOTS is slower than other non-ODE methods; however, we argue that this is an implementation issue. Clearly, Neural ODEs received much less attention than State-Space Models, Transformers or RNNs. We use the TorchODE library (Lienen & Günnemann, 2022). Although it is faster than the original implementation (Chen et al., 2018), it still requires work, being built almost single-handedly by its main contributor.

Backpropagation is done via the AutoDiff method, which is faster than Adjoint backpropagation. However, it is also more memory-consuming. We fix the tolerance to 10^{-3} and use the adaptive Dopri5 solver. The normalizing constant (4) is set to the median size of the timeframe across the dataset. Our version of cubic spline interpolation skips NaN values, interpolating only between present ones. All-zero channels are set to a constant zero. All our model versions use the GRU Cell as their dynamics function:

- For no negative feedback, we use the GRU as-is;
- To add our adaptive version from (2), we pass $-\mathbf{h}$ instead of \mathbf{h} to a standard PyTorch GRU.
- For the constant version (3), we subtract the current hidden from the derivative.

GRU turns out to be a surprisingly convenient framework for incorporating negative feedback. While other architectures are possible, they do not allow for such an elegant approach: one would have to manually add a learnable sigmoid-RNN layer for the mechanism to be adaptive.

Mamba. The Mamba model that we use is Mamba2 from the Mamba SSM library ², which we employ without significant modifications.

Neural CDE. To reproduce the results as closely as possible, we use TorchCDE ³ for the Neural CDE method. Specifically, we implemented the example for irregular sequence classification from their repository.

B.3. Datasets

Below is a detailed description of each dataset:

- The PhysioNet Sepsis ⁴ dataset (Reyna et al., 2020). Most of the values are missing, with only 10% present. Sequences are rather short, ranging from 8 to 70 elements, with a median length of 38. The target variable indicates whether the patient developed sepsis, meaning it’s binary and highly unbalanced, so we measure AUROC. This dataset is also used by the original NCDE paper (Kidger et al., 2020), making it a valuable addition to our benchmark. Following the NCDE paper, we only consider the first 72 hours of a patient’s stay.
- The WISDM Human Activity Recognition ⁵ dataset (Weiss, 2019). It contains evenly-spaced physical coordinates

¹https://anonymous.4open.science/status/denots_icml2025-BB26

²<https://github.com/state-spaces/mamba>

³<https://github.com/patrick-kidger/torchcde>

⁴<https://physionet.org/content/challenge-2019/1.0.0/>

⁵<https://archive.ics.uci.edu/dataset/507/wisdm+smartphone+and+smartwatch+activity+and+biometrics+dataset>

and acceleration data. Each sequence is 3 minutes long, with observations occurring 4 times per second, totalling 720 elements per sequence (we resampled it from 20Hz to keep sequence lengths reasonable). Additionally, this dataset contains a mere 809 elements, making it useful to test models for overfitting. The target is multiclass, with 18 classes.

- A synthetic Pendulum dataset, with the dampening coefficient as the target (Osin et al., 2024). Sequences are irregular, containing 10% missing values, with lengths varying from approximately 200 to 400 elements, the median length being 315. We provide the code to generate this dataset in our repository.

This choice of datasets allows us to test the considered models in multiple challenging areas: on long sequences, on irregular sequences, and sequences with many missing values and scarce data.

B.4. Pipeline

We provide our repository with automated scripts to download and preprocess all datasets, as well as to train and evaluate all the considered models, using popular frameworks such as Pytorch (Ansel & team, 2024), Pytorch Lightning (Falcon & The PyTorch Lightning team, 2019) and Hydra (Yadan, 2019) to make the process familiar to most AI researchers. The YAML-configs, containing all the hyperparameters, are also provided in the repository to facilitate reproducibility.

B.4.1. TRAINING

All training uses the Adam method (Kingma, 2014), with the learning rate fixed to 10^{-3} . The whole model, consisting of the head and the backbone, is trained end-to-end. The head consists of a linear layer and an activation function. We do not set an upper bound for epochs, stopping only when the validation metric stops improving. The choice of head’s activation, loss and specific metrics depend on the considered task, as outlined in Table 3.

| Task | Activation | Loss | Metric |
|------------|------------|----------------------|----------|
| Regression | - | Mean squared error | R^2 |
| Binary | Sigmoid | Binary cross-entropy | AUROC |
| Multiclass | Softmax | Cross-entropy | Accuracy |

Table 3. Head activation, loss and metric choice for each considered downstream task.

B.4.2. EMBEDDINGS

Before passing $\{\mathbf{x}_k\}_k$ to the backbone, we apply Batch Normalization (Ioffe & Szegedy, 2015), but with the affine parameters turned off to standardize the input features. For a fairer baseline comparison, time intervals $t_k - t_{k-1}$ are also included in the embeddings in the same way as other numerical features.

For the Sepsis dataset, the considered numerical features represent medical variables and are thus presumably more complex than the physical coordinate/acceleration data from the other two datasets. To account for this, we inflate each of them to a dimension of 100 using a trainable linear layer before the backbone. Besides, this dataset has static features, which we use as the starting points where applicable.

The NaN values for the models which do not support missing values were replaced via forward/backward filling.

B.5. Attacks

The attacks from Section 4.2 were each repeated for 10 different seeds and then averaged over. Using this, we also provide the variance via tinting in Figure 4.

B.6. Dataset choice

Depth expressiveness. To test our overfitting hypothesis, we required a small version of one of the datasets. The Pendulum dataset fits perfectly since it has a regression target, meaning that any small subset would be balanced. Moreover, it is synthetic, so we can modify it as we see fit.

Negative feedback ablation. For our negative feedback study, we needed a dataset that would allow us to test our model’s expressiveness to the full extent. Sepsis is the only dataset that is both real and has enough samples so methods do not

overfit.

Attacks All our attacks were conducted on the HAR dataset. This dataset is the only one of the three that does not contain any NaNs. That means we can add Gaussian noise anywhere and replace any subset of the observations with NaNs.

B.7. Results

B.7.1. FULL VERSION OF METRICS

To save space, we only provided the mean metric scores of the considered models and did not display the variance. Table 4 gives the full picture.

| Backbone | HAR Accuracy | Pendulum R^2 | Sepsis AUROC |
|-------------------|-----------------------------------|-----------------------------------|-----------------------------------|
| RNN | 0.38 ± 0.02 | 0.49 ± 0.42 | 0.86 ± 0.01 |
| Transformer | 0.39 ± 0.05 | 0.57 ± 0.06 | 0.78 ± 0.21 |
| Mamba | 0.28 ± 0.03 | 0.58 ± 0.02 | 0.85 ± 0.02 |
| NCDE | \times | -0.36 ± 0.16 | 0.88 ± 0.01 |
| DeNOTS-1 (No NF) | 0.47 ± 0.04 | 0.47 ± 0.01 | 0.90 ± 0.01 |
| DeNOTS-10 (No NF) | 0.15 ± 0.04 | \times | 0.45 ± 0.02 |
| DeNOTS-20 (No NF) | 0.15 ± 0.05 | \times | 0.44 ± 0.01 |
| DeNOTS-1 | 0.48 ± 0.05 | 0.44 ± 0.01 | 0.91 ± 0.00 |
| DeNOTS-10 | 0.39 ± 0.02 | 0.63 ± 0.04 | 0.93 ± 0.00 |
| DeNOTS-200 | 0.43 ± 0.03 | 0.64 ± 0.04 | 0.93 ± 0.01 |

Table 4. Full metrics with standard deviation.

B.7.2. BASELINES DISCUSSION

Mamba and the Transformer show good, stable quality. The Neural CDE Sepsis results are taken directly from (Kidger et al., 2020) and also compare well with others. However, the method performed abysmally on Pendulum and did not converge at all on HAR. RNN, on the other hand, performs well on HAR and Sepsis; however, it has very high variance on the long-sequence Pendulum dataset, oftentimes learning to simply predict the average target, unable to surpass $R^2 = 0$. This is likely due to the nature of the task. Predicting the dampening coefficient requires memorizing several oscillation cycles, and GRU, albeit better than simple RNNs, still does not have good enough long-term memory. This is further supported by the fact that both Mamba and the Transformer achieve high quality on this task: they have no such memory issue.

To test these hypotheses, we also conduct experiments on a shortened version of the Pendulum dataset, with a fourfold reduction of sequence lengths. Note that the total time and oscillation frequency remain the same, so cycles happen more quickly element-wise. The results are presented in Table 5. Clearly, reducing sequence length stabilises Neural CDE and allows RNN to learn inter-cycle dynamics more easily.

| Backbone | Test R^2 | Original R^2 |
|----------|-----------------|------------------|
| RNN | 0.59 ± 0.02 | 0.49 ± 0.42 |
| NCDE | 0.37 ± 0.13 | -0.36 ± 0.16 |

Table 5. Experiments on a shorter version of the Pendulum dataset. For convenience, we also provide the original R^2 scores.